

MHD Free-Convection from a Rotating Vertical Plate with Power-law Variation

M. Wahiduzzaman^{*1}, Gopal Chandra Mazumder², A. Sarker³ and M.S. Uddin⁴

^{1,3,4}Mathematics Discipline, Khulna University, Khulna-9208, Bangladesh

²Upazilla Secondary Education Officer, Directorate of Secondary and Higher Education
Ministry of Education, Chougacha, Jessore, Bangladesh.

*Corresponding author's email: wahidmathku@gmail.com

Received 19 October 2014; accepted 1 November 2014

Abstract. Effects of viscous dissipation and joule heating on MHD-free convection flow of an electrically conducting fluid bounded by a rotating semi-infinite vertical plate in the presence of the combined effect of Hall and ion-slip currents at surface temperature will be investigated. Also, a strong transverse magnetic field is imposed perpendicularly to the plate on the fluid. The governing equations of this problem contain the nonlinear coupled partial differential equations. Firstly the governing differential equations are transformed into similar ordinary coupled and non-linear equations by introducing proper non-similarity variables and solved numerically using Nactsheim-Swigert shooting iteration technique. The effects of various parameters on the velocity and temperature profiles as well as the local shear stresses and the local Nusselt number are presented graphically.

Keywords: MHD, Joule heating, Hall current, Ion-Slip current, rotating system

1. Introduction

Magneto hydro-dynamic free convection flow of an electrically conducting fluid along a heated semi-infinite vertical flat plate in the presence of a strong magnetic field has been studied by Sparrow and Cess [1]. In this study, Hall and ion-slip terms were ignored in applying Ohm's law as it has no marked effect for small and moderate values of the magnetic field. However, the current trend for the application of magneto-hydrodynamic is towards a strong magnetic field, so that the influence of the electromagnetic force is noticeable. Under these conditions Hall and Ion-slip currents are important and they have a marked effect on the magnitude and direction of the current density and consequently on the magnetic force term. The problem of MHD free convection flow with Hall and ion-slip currents has many important engineering applications, e.g. in power generators, Hall accelerators and flows in channels and ducts. Hossain M.A [2] studied the effect of viscous and Joule heating on the flow of an electrically conducting, viscous, incompressible fluid past a semi-infinite plate with surface temperature varying linearly with the distance from the leading edge in the presence of a uniform transverse magnetic field. Abo-Eldahab and El Aziz [3] have studied viscous dissipation and joule heating effects on MHD-free convection from a vertical plate with power-law variation in surface temperature in the presence of Hall and ion-slip currents and the derived fundamental equations are solved numerically. But the rotating plate have not considered in [3].

M. Wahiduzzaman, Gopal Chandra Mazumder, A. Sarker and M.S. Uddin

Kutub Uddin et. al. (2012)[4] studied the Radiation-conduction Interaction with Steady streamwise surface temperature variations over a vertical cone. Haque et. al. investigate the Ekman boundary layer mixed convective heat transfer flow through a porous medium with large suction. Saidul Islam studied the MHD Free Convection and Mass Transfer Flow with Heat Generation through an Inclined Plate.

Our aim is to study the effects of viscous dissipation and joule heating on MHD-free convection flow of an electrically conducting fluid bounded by a rotating semi-infinite vertical plate in the presence of the combined effect of Hall and ion-slip currents at surface temperature.

2. Governing equation

Consider a steady, laminar, incompressible, free convection boundary layer flow of an electrically conducting and heat generating/absorption fluid along a vertical semi-infinite rotating plate with the origin at the leading edge.

Let x and y axes are parallel and normal, respectively, and let the z axis be coincident with the leading edge of the plate. The surface temperature on the heated plate is assumed to vary according to the power-law form, $T_w = T_\infty + Ax^n$, where A is constant and n is exponent. An external strong magnetic is applied in the y -direction and has a constant flux density \mathbf{B}_0 . The magnetic Reynolds number of the flow is taken to be small enough so that the induced distortion of the applied magnetic field can be neglected.

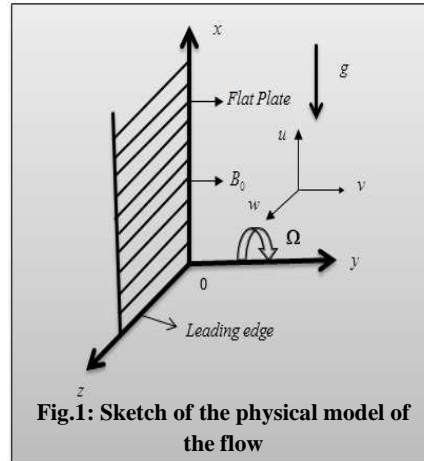


Fig.1: Sketch of the physical model of the flow

The electron-atom collision frequency is assumed to be relatively high, so that the Hall and ion-slip effects cannot be neglected. The effect of Hall current gives rise to a force in the z -direction, which induces cross flow in that direction, and hence the flow becomes three-dimensional. To simplify the analysis, we assume that there is no variation of flow and heat transfer quantities in the z -direction, which is valid if the plate would be of infinite width in this direction. Assuming the plate to be electrically non-conducting, the generalized Ohm's law gives $J_y = 0$ everywhere in the flow. The governing equations for this investigation are modified to include viscous and Joule heating effects with the generalized Ohm's and Maxwell's laws. With the usual boundary layer and Boussinesq approximations the problem is governed by the following equations;

The Continuity equation;

$$\frac{\partial u}{\partial x} + \frac{\partial v}{\partial y} = 0 \quad (1)$$

Momentum equation in x -direction;

MHD Free-Convection from a Rotating Vertical Plate with Power-law Variation

$$\frac{\partial u}{\partial t} + u \frac{\partial u}{\partial x} + v \frac{\partial u}{\partial y} = \nu \left(\frac{\partial^2 u}{\partial y^2} \right) + g\beta(T - T_\infty) + 2w\Omega - \frac{B^2 \sigma_e}{\rho(\alpha_e^2 + \beta_e^2)} [\alpha_e u + \beta_e w] \quad (2)$$

Momentum equation in z -direction;

$$\frac{\partial w}{\partial t} + u \frac{\partial w}{\partial x} + v \frac{\partial w}{\partial y} = \nu \left(\frac{\partial^2 w}{\partial y^2} \right) - 2u\Omega + \frac{B^2 \sigma_e}{\rho(\alpha_e^2 + \beta_e^2)} [\beta_e u - \alpha_e w] \quad (3)$$

Energy equation;

$$\frac{\partial T}{\partial t} + u \frac{\partial T}{\partial x} + v \frac{\partial T}{\partial y} = \frac{k}{\rho C_p} \left(\frac{\partial^2 T}{\partial y^2} \right) + \frac{Q}{\rho C_p} (T - T_\infty) + \frac{\mu}{\rho C_p} \left[\left(\frac{\partial u}{\partial y} \right)^2 + \left(\frac{\partial w}{\partial y} \right)^2 \right] + \frac{\sigma_e B_0^2}{\rho C_p (\alpha_e^2 + \beta_e^2)} (u^2 + w^2) \quad (4)$$

with the corresponding initial and boundary conditions are

$$\left. \begin{aligned} u \rightarrow 0, w \rightarrow 0, T \rightarrow T_\infty & \quad \text{at } x=0, y > 0 \\ u = 0, v = 0, w = 0, T = T_w(x) = T_\infty + Ax^n & \quad \text{at } y=0, x > 0 \\ u \rightarrow 0, w \rightarrow 0, T \rightarrow T_\infty & \quad \text{at } y \rightarrow \infty \end{aligned} \right\} \quad (5)$$

where (u, v, w) are the velocity components along the (x, y, z) axes, respectively, T be the fluid temperature, σ_e is the electrical conductivity, e is the electron charge. ρ, ν and C_p are the density, kinematic viscosity and specific heat at constant pressure of the fluid, respectively. β, Q, g and k are the coefficient of thermal expansion, volumetric rate of heat generation, acceleration due to gravity and thermal conductivity, respectively, $\alpha_e = 1 + \beta_i \beta_e$, β_e and β_i are Hall and Ion-slip currents.

3. Mathematical formulation

In order to solve Equations (1)-(4) under the boundary conditions (5), we adopt the well-defined similarity analysis to attain similarity solutions. For this purpose, the following similarity transformations are now introduced;

$$\eta = Cyx^{\frac{-1}{4}}, \quad \xi = x^{\frac{1}{2}} L^{\frac{-1}{2}}, \quad \psi = 4\nu Cx^{\frac{3}{4}} f(\xi, \eta)$$

$$w = 4\nu C^2 x^{\frac{1}{2}} g(\xi, \eta), \quad \theta = \frac{T - T_\infty}{T_w(x) - T_\infty}, \quad C = \left(\frac{g\beta[T_w(x) - T_\infty]}{4\nu^2} \right)^{\frac{1}{4}} \quad (6)$$

$$M = \frac{\sigma B_0^2 L^{\frac{1}{2}}}{2\rho\nu C^2}, \quad P_r = \frac{\nu\rho c_p}{k}, \quad E_c = \frac{gBL}{c_p}, \quad \gamma = \frac{QL^{\frac{1}{2}}}{2\rho c_p \nu C^2}$$

The continuity equation is satisfied by

$$u = \frac{\partial \psi}{\partial y} \quad \text{and} \quad v = -\frac{\partial \psi}{\partial x} \quad (7)$$

M. Wahiduzzaman, Gopal Chandra Mazumder, A. Sarker and M.S. Uddin

$$u = 4\nu Cx^{-\frac{1}{2}} f'(\xi, \eta) \quad \text{and} \quad v = -\nu Cx^{-\frac{1}{4}} \left\{ (n+3)f(\xi, \eta) + 2\xi \frac{\partial f}{\partial \xi} + (n-1)f'(\xi, \eta) \right\} \quad (8)$$

Using the above equations (6 to (8), we can show that the equations (1)-(4) reduce to the below form

Hence the reduced equations are

$$f''' + (n+3)ff'' - 2(n+1)f'^2 + \theta - \frac{2M\xi}{\alpha_e^2 + \beta_e^2}(\alpha_e f' + \beta_e g) + Rg = 2\xi \left(f' \frac{\partial f'}{\partial \xi} - f'' \frac{\partial f}{\partial \xi} \right) \quad (9)$$

$$g'' - 2(n+1)f'g + (n+3)fg' - \frac{2M\xi}{\alpha_e^2 + \beta_e^2}(\alpha_e g - \beta_e f') - Rf' = 2\xi \left(f' \frac{\partial g}{\partial \xi} - g' \frac{\partial f}{\partial \xi} \right) \quad (10)$$

$$\frac{1}{p_r} \theta'' + (n+3)f\theta' - 4nf'\theta + 2\xi\gamma\theta + 4\xi^2 E_c (f''^2 + g''^2) + \frac{8ME_c\xi^3}{\alpha_e^2 + \beta_e^2} (f'^2 + g'^2) = 2\xi \left(f' \frac{\partial \theta}{\partial \xi} - \theta' \frac{\partial f}{\partial \xi} \right) \quad (11)$$

and the corresponding boundary conditions become

$$\text{at } \eta = 0 \quad f'(\xi, 0) = 0, \quad 3f(\xi, 0) + 2\xi \frac{\partial f(\xi, 0)}{\partial \xi} = 0, \quad g(\xi, 0) = 0, \quad \theta(\xi, 0) = 1 \quad (12)$$

$$\text{at } \eta = \infty \quad f'(\xi, \infty) = 0, \quad g(\xi, \infty) = 0, \quad \theta(\xi, \infty) = 0$$

(13) Also, the Skin-friction coefficient may be written as follows:

$$\therefore h(x) = -kCx^{-\frac{1}{4}} \theta'(\xi, 0) \quad (14)$$

The rate of heat transfer is given by

$$\therefore Nu_x = \frac{1}{\sqrt{2}} (Gr_x)^{\frac{1}{4}} \theta'(\xi, 0) \quad (15)$$

4. Numerical technique

The set of nonlinear ordinary differential equations (9) to (11) with boundary conditions (12)-(13) were solved numerically using Nachtshein-Swigert iteration technique with a systematic guessing of $f''(0)$, $g'(0)$ and $\theta'(0)$ by the shooting technique until the boundary conditions at infinity $f'(0)$, $g(0)$ and $\theta(0)$ decay exponentially to zero. The step size $\Delta\eta = 0.01$ is used while obtaining the numerical solution with η_{\max} , and accuracy to the fifth decimal place is sufficient for convergence. A step size of $\Delta\eta = 0.01$ was selected to be satisfactory for a convergence criterion of 10^{-7} in nearly all cases. The maximum value of η_{∞} , to each group of parameter α, γ, M^2 and m determined when the values of unknown boundary conditions at $\eta = 0$ not change to successful loop with error less than 10^{-7} . Effects of chemical reaction, heat and mass transfer on nonlinear MHD boundary layer flow over a porous shrinking sheet is studied in the presence of suction. In the following section, the results are discussed in details.

5. Results and discussion

The governing boundary layer equations (9) to (11) subject to the boundary conditions (12)-(13) are approximated by a system of non-linear ordinary differential equations replacing the derivatives with respect to ξ by two-point back ward finite difference with step size 0.01. The results of the numerical computations are displayed in Figs. 2–19. For the change of magnetic parameter (M), the primary velocity decreases, secondary velocity and temperature distributions have been illustrated in Figure 2-4. From these figures it has been observed that the primary velocity decreases as the increasing values of the magnetic parameter and the Secondary velocity increases with the increase of magnetic parameter and there are minor effects in temperature distribution. For the change of Eckert number (E_c), the primary, secondary velocity and temperature distributions have been illustrated in Figs 5-7, where secondary velocity and the temperature distribution with the increases of Eckert number. From Figs 8-10, it has been observed that the primary velocity and secondary velocity decreases with the increase of rotational parameter and temperature distribution with the increasing values of rotational parameter and the secondary velocity decreases with the increase of rotational parameter. For the change of hall parameter β_e , the primary, secondary velocity and temperature distributions have been illustrated in Figs 11-13. From these figures it has been observed that there are minor effects in the primary velocity but small increment and temperature distribution with the increasing values of hall parameter parameter and the secondary velocity decreases with the increase of hall parameter. For the change of ion-slip parameter β_i , the primary, secondary velocity and temperature distributions have been illustrated in Figs 13-15. From these figures it has been observed that there are minor effects in the primary velocity but small decrement and temperature distribution with the increasing values of ion-slip parameter and the secondary velocity increases with the increase of ion-slip parameter. For the change of heat absorption parameter γ , the primary, secondary velocity and temperature distributions have been illustrated in Figs 17-19. From these figures it has been observed that the primary velocity distribution is increasing with the increase o heat absorption parameter and there are minor effects in temperature distribution with the increasing values of heat absorption parameter and the secondary velocity decreases with the increase of rotational parameter. From Figs 20-22, it has been observed that the primary velocity and the secondary velocity increases with the increase of temperature power coefficient but temperature are decreases with increasing values of the temperature power coefficient number. For the change of Prandlt number (P_r), the primary, secondary velocity and temperature distributions have been illustrated in Figs 23-25. From these figures it has been observed that the primary velocity and temperature are decreased as the increasing values of the Prandlt number and the Secondary velocity increases with the increase of Prandlt number.

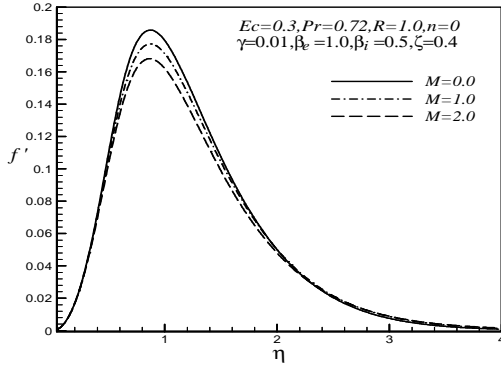


Figure 2: Primary velocity profile for Magnetic parameter.

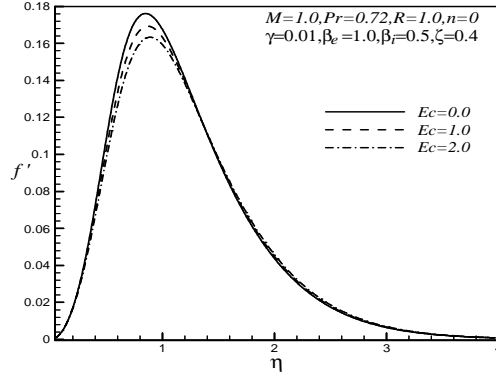


Figure 5: Primary velocity profile for Rotational parameter.

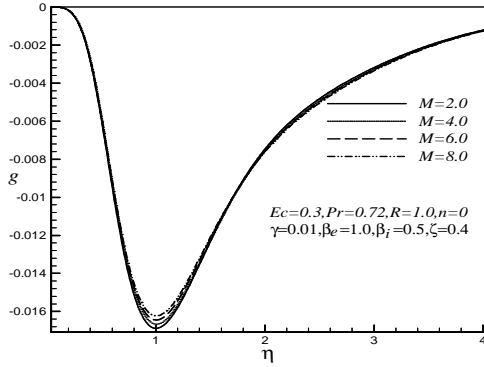


Figure 3: Secondary velocity profile for Magnetic parameter.

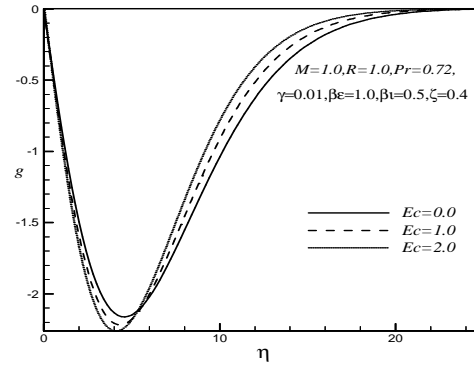


Figure 6: Secondary velocity profile for Rotational parameter.

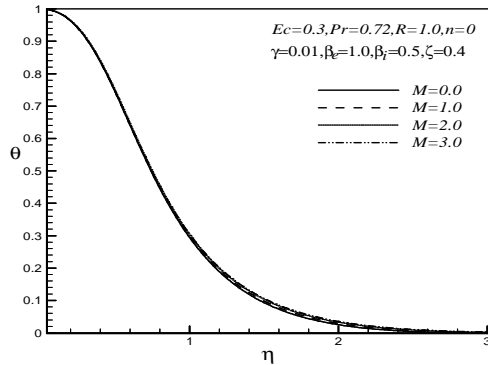


Figure 4: Temperature profile for Magnetic parameter.

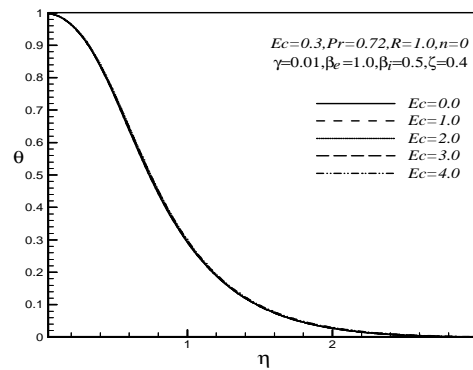


Figure 7: Temperature profile for Rotational parameter.

MHD Free-Convection from a Rotating Vertical Plate with Power-law Variation

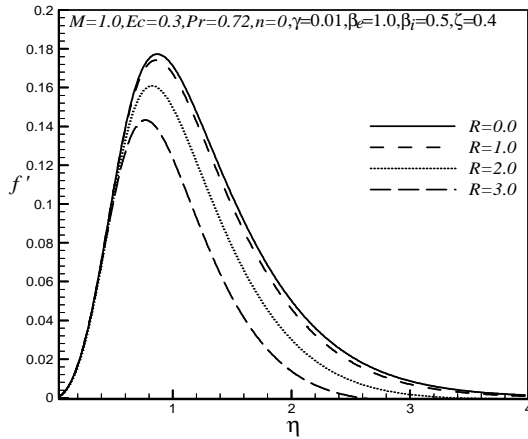


Figure 8 Primary velocity profile for Eckert number.

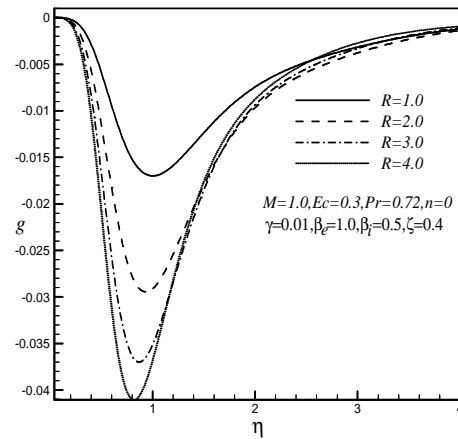


Figure 9: Secondary velocity profile for Eckert number

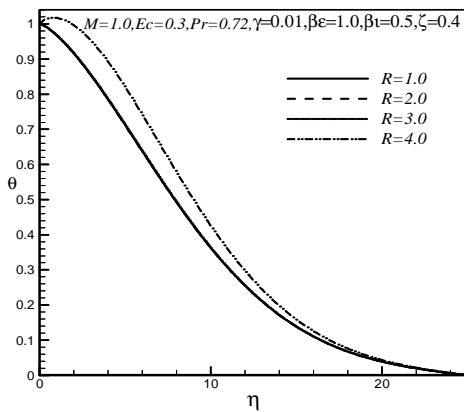


Fig. 10: Temperature profile for Eckert number.

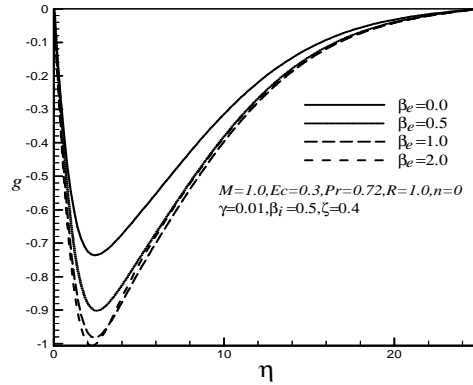


Fig. 12: Secondary velocity profile for Hall parameter.

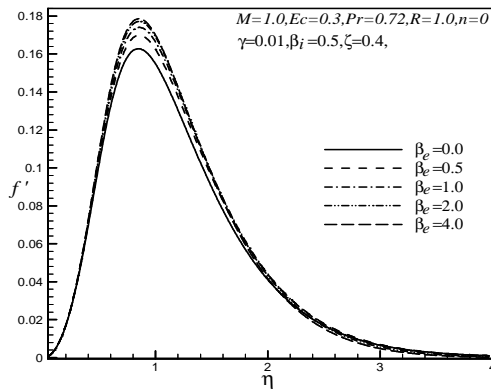


Fig. 11: Primary velocity profile for Hall parameter.

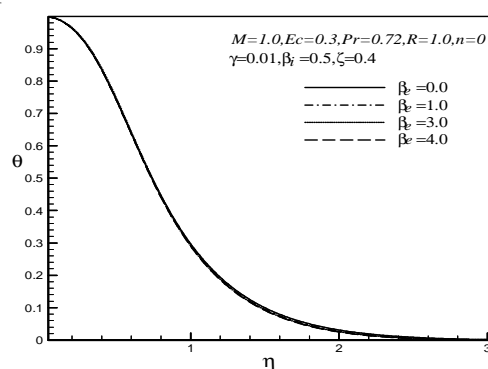


Fig. 13: Temperature profile for Hall parameter.

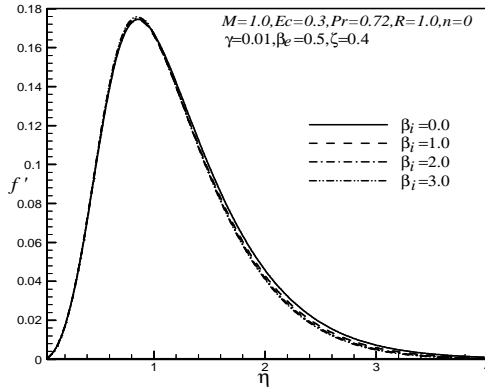


Fig. 14: Primary velocity profile for Ion-slip parameter.

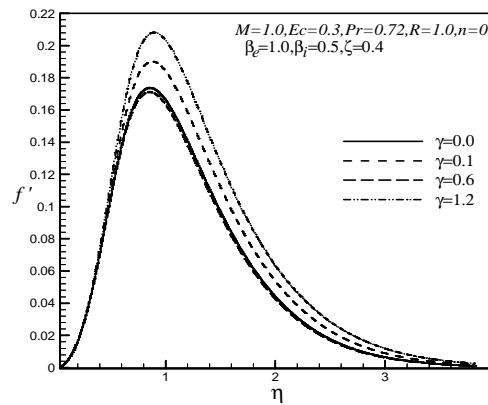


Fig. 17: Primary velocity profile for heat absorption coefficient.

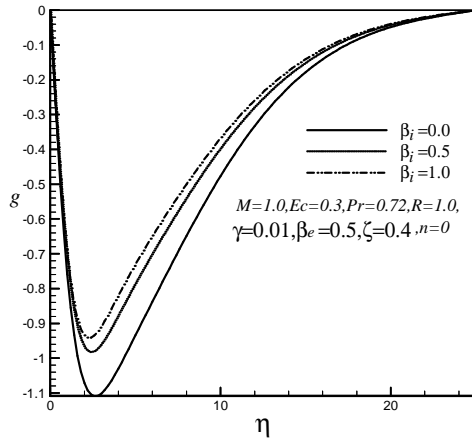


Fig. 15: Secondary velocity profile for Ion-slip parameter.

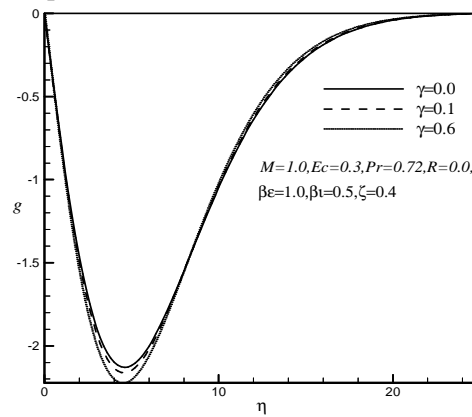


Fig. 18 Secondary velocity profile for heat absorption coefficient

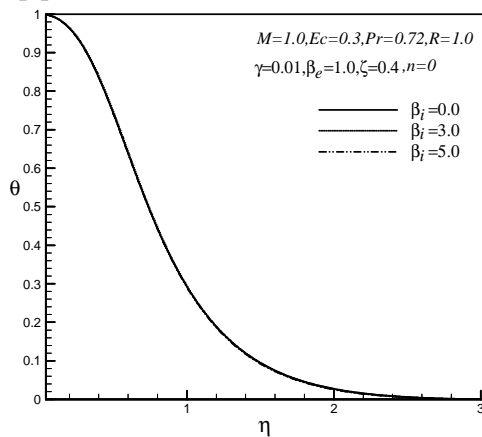


Fig. 16: Temperature profile for Ion-slip parameter.

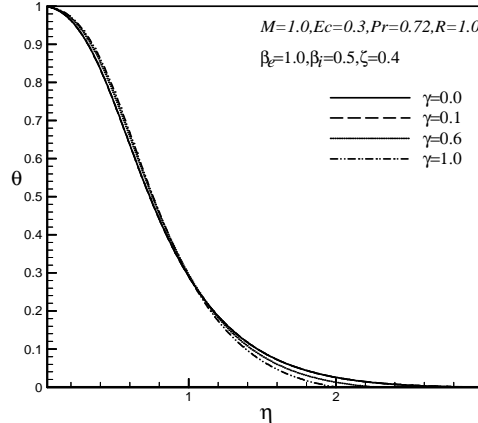


Fig. 19: Temperature profile for heat absorption coefficient.

MHD Free-Convection from a Rotating Vertical Plate with Power-law Variation

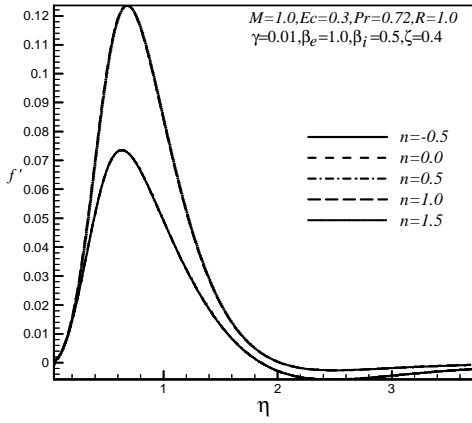


Fig. 20: Primary velocity profile for temperature power coefficient.

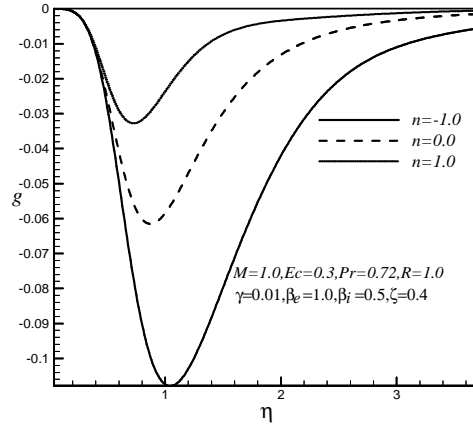


Fig. 21: Secondary velocity profile for temperature power coefficient.

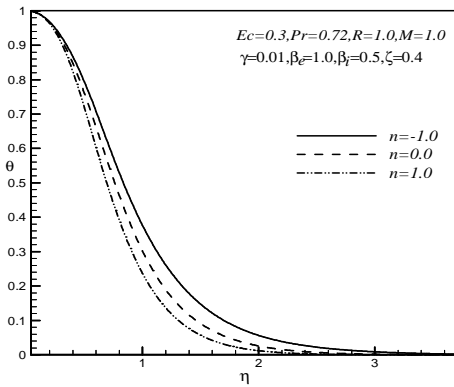


Fig. 22: Temperature profile for temperature power coefficient.

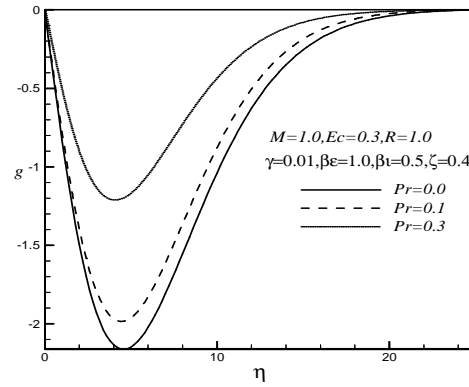


Fig. 24: Secondary velocity profile for Prandtl number.

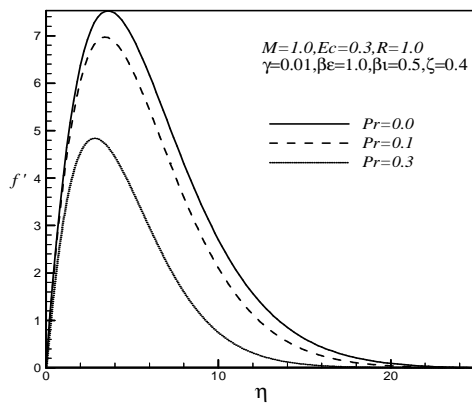


Fig. 23: Primary velocity profile for Prandtl number.

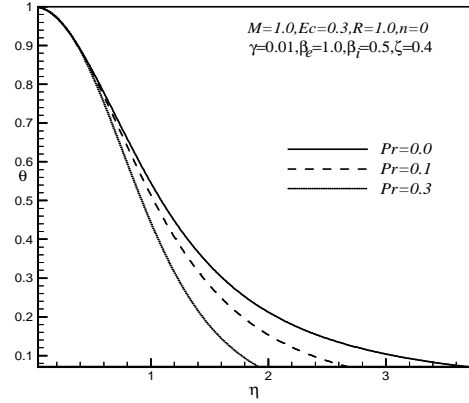


Fig. 25: Temperature profile for Prandtl number.

M. Wahiduzzaman, Gopal Chandra Mazumder, A. Sarker and M.S. Uddin

Since the physical interest of the problem, the dimensionless skin-friction coefficient $(-f'')$, in x -direction, skin-friction coefficient $(-g')$ in z -direction and the dimensionless heat transfer rate $(-\theta')$ are plotted against heat source parameter γ and illustrated in Fig. 26-45. For the change of magnetic parameter (M), the skin-friction coefficient $(-f'')$ along x -direction, the skin-friction coefficient $(-g')$ along z -direction and the dimensionless heat transfer rate $(-\theta')$ are plotted against heat source parameter γ for the different values of Magnetic parameter M where $P_r = 0.72$, $R = 1.0$, $E_c = 0.3$, $\beta_i = 0.5$, $\beta_e = 1.0$, $n = 0.0$, $\gamma = 0.01$ and $\xi = 0.4$ illustrated in Fig. 25-4.6.26. From these figures it has been observed that the skin-friction coefficient $(-f'')$ along x -direction decreases as the increasing values of the magnetic parameter and the skin-friction coefficient $(-g')$ along z -direction increases with the increase of magnetic parameter but there is a minor effect in the dimensionless heat transfer rate $(-\theta')$. For the change of Eckert number (E_c), the skin-friction coefficient $(-f'')$ along x -direction, the skin-friction coefficient $(-g')$ along z -direction and the dimensionless heat transfer rate $(-\theta')$ are plotted against heat source parameter γ for the different values of Eckert number (E_c) where $P_r = 0.72$, $R = 1.0$, $M = 1.0$, $\beta_i = 0.5$, $\beta_e = 1.0$, $n = 0.0$, $\gamma = 0.01$ and $\xi = 0.4$ illustrated in Fig. 28-29. From these figures it has been observed that the skin-friction coefficient $(-f'')$ along x -direction decreases as the increasing values of the Eckert number. But the skin-friction coefficient $(-g')$ along z -direction and the dimensionless heat transfer rate $(-\theta')$ have minor effects as the increasing values of the Eckert number. For the change of rotational parameter (R), the skin-friction coefficient $(-f'')$ along x -direction, the skin-friction coefficient $(-g')$ along z -direction and the dimensionless heat transfer rate $(-\theta')$ are plotted against heat source parameter γ for the different values of rotational parameter where $P_r = 0.72$, $M = 1.0$, $E_c = 0.3$, $\beta_i = 0.5$, $\beta_e = 1.0$, $n = 0.0$, $\gamma = 0.01$ and $\xi = 0.4$ illustrated in Fig. 29-31. From these figures it has been observed that the skin-friction coefficient $(-f'')$ along x -direction and the skin-friction coefficient $(-g')$ along z -direction decrease as the increasing values of the rotational parameter but the dimensionless heat transfer rate $(-\theta')$ increases. For the change of heat absorption

MHD Free-Convection from a Rotating Vertical Plate with Power-law Variation

parameter γ , the skin-friction coefficient $(-f'')$ along x -direction, the skin-friction coefficient $(-g')$ along z -direction and the dimensionless heat transfer rate $(-\theta')$ are plotted against heat source parameter γ for the different values of heat absorption parameter γ where $P_r = 0.72$, $R = 1.0$, $E_c = 0.3$, $\beta_i = 0.5$, $\beta_e = 1.0$, $n = 0.0$, $M = 1.0$ and $\xi = 0.4$ illustrated in Fig.33-35. From these figures it has been observed that the skin-friction coefficient $(-f'')$ along x -direction and the skin-friction coefficient $(-g')$ along z -direction decreases as the increasing values of the heat absorption parameter but the dimensionless heat transfer rate $(-\theta')$ increases with the increase of heat absorption parameter. For the change of hall parameter β_e , the skin-friction coefficient $(-f'')$ along x -direction, the skin-friction coefficient $(-g')$ along z -direction and the dimensionless heat transfer rate $(-\theta')$ are plotted against heat source parameter γ for the different values of hall parameter β_e where $P_r = 0.72$, $R = 1.0$, $E_c = 0.3$, $\beta_i = 0.5$, $M = 1.0$, $n = 0.0$, $\gamma = 0.01$ and $\xi = 0.4$ illustrated in Fig. 36-37. From these figures it has been observed that the skin-friction coefficient $(-f'')$ along x -direction has no decision as the increasing values of the hall parameter and the skin-friction coefficient $(-g')$ along z -direction decreases with the increase of hall parameter and there are minor effects in the dimensionless heat transfer rate $(-\theta')$. For the change of ion-slip parameter β_i , the skin-friction coefficient $(-f'')$ along x -direction, the skin-friction coefficient $(-g')$ along z -direction and the dimensionless heat transfer rate $(-\theta')$ are plotted against heat source parameter γ for the different values of ion-slip parameter β_i where $P_r = 0.72$, $R = 1.0$, $E_c = 0.3$, $M = 1.0$, $\beta_e = 1.0$, $n = 0.0$, $\gamma = 0.01$ and $\xi = 0.4$ illustrated in Fig. 38-39. From these figures it has been observed that the skin-friction coefficient $(-f'')$ along x -direction and the dimensionless heat transfer rate $(-\theta')$ have minor effects as the increasing values of the ion-slip parameter and the skin-friction coefficient $(-g')$ along z -direction have no decision with the increase of ion-slip parameter

For the change of temperature power coefficient (n) the skin-friction coefficient $(-f'')$ along x -direction, the skin-friction coefficient $(-g')$ along z -direction and the dimensionless heat transfer rate $(-\theta')$ are plotted against heat source parameter γ for

M. Wahiduzzaman, Gopal Chandra Mazumder, A. Sarker and M.S. Uddin

temperature power coefficient (n) where $P_r = 0.72$, $R = 1.0$, $E_c = 0.3$, $M = 1.0$, $\beta_e = 1.0$, $\beta_i = 0.5$, $\gamma = 0.01$ and $\xi = 0.4$ illustrated in Fig. 40-42. From these figures it has been observed that the skin-friction coefficient ($-f''$) along x -direction and the dimensionless heat transfer rate ($-\theta'$) decrease as the increasing values of temperature power coefficient. And the skin-friction coefficient ($-g'$) along z -direction increases as the increasing values of temperature power coefficient. For the change of Prandtl number (P_r), the skin-friction coefficient ($-f''$) along x -direction, the skin-friction coefficient ($-g'$) along z -direction and the dimensionless heat transfer rate ($-\theta'$) are plotted against heat source parameter γ for the different values of Prandtl number where $P_r = 0.72$, $R = 1.0$, $E_c = 0.3$, $\beta_i = 0.5$, $\beta_e = 1.0$, $n = 0.0$, $\gamma = 0.01$ and $\xi = 0.4$ illustrated in Fig. 43-45. From these figures it has been observed that the skin-friction coefficient ($-f''$) along x -direction and the dimensionless heat transfer rate ($-\theta'$) decrease as the increasing values of Prandtl number but the skin-friction coefficient ($-g'$) along z -direction increases as the increasing values of Prandtl number.

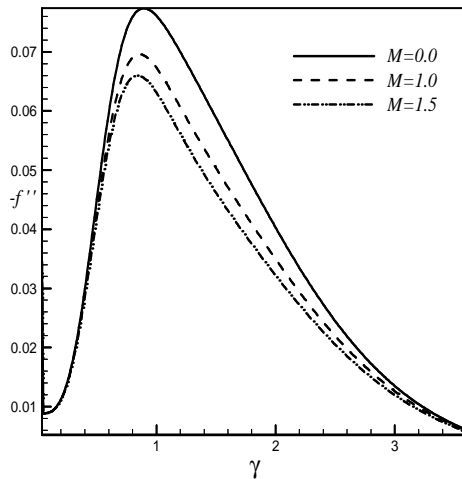


Fig. 26: Effect of M on Skin friction coefficient in x -direction.

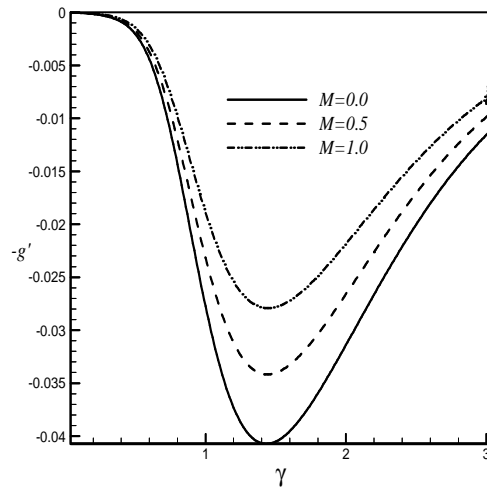


Fig. 27: Effect of M on Skin friction coefficient in z -direction.

MHD Free-Convection from a Rotating Vertical Plate with Power-law Variation

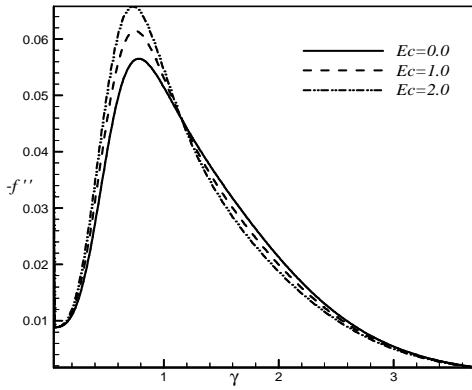


Fig. 28: Effect of E_c on Skin friction coefficient in x -direction.

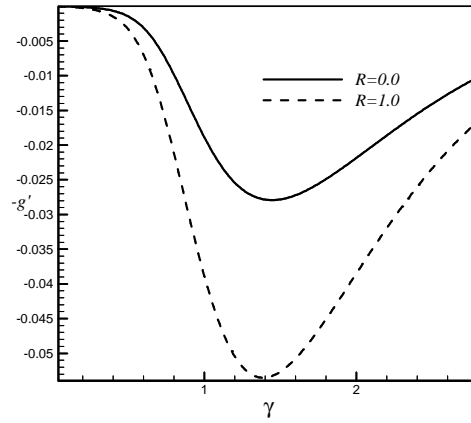


Fig. 31: Effect of R on Skin friction coefficient in z -direction.

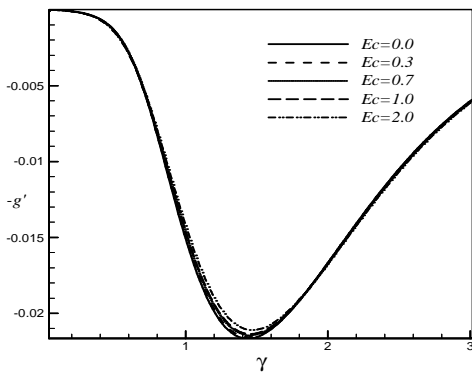


Fig. 29: Effect of E_c on Skin friction coefficient in z -direction.

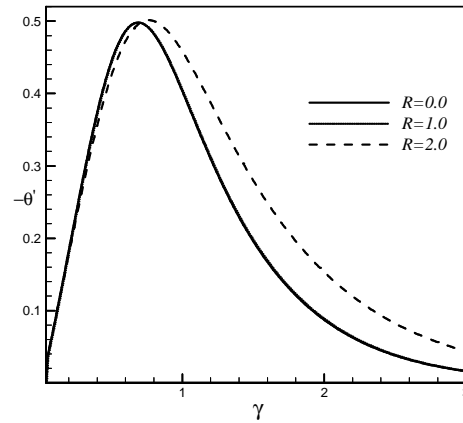


Fig. 32: Effect of R on the rate of heat transfer.

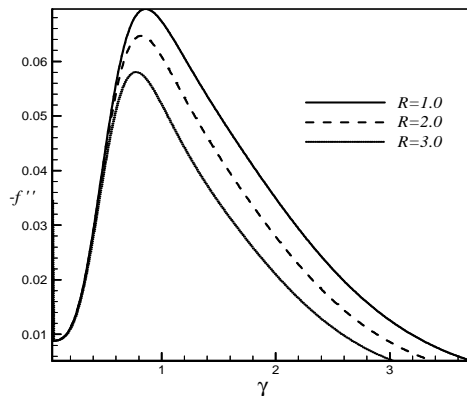


Fig. 30: Effect of R on Skin friction coefficient in x -direction.

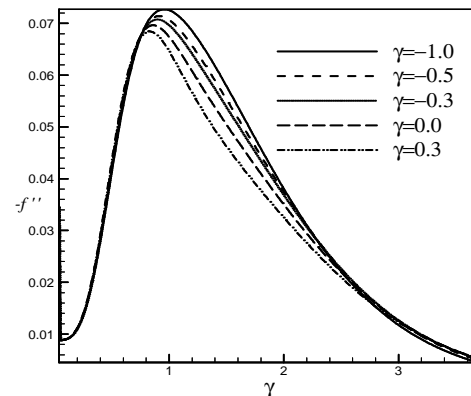


Fig. 33: Effect of γ on Skin friction coefficient in x -direction.

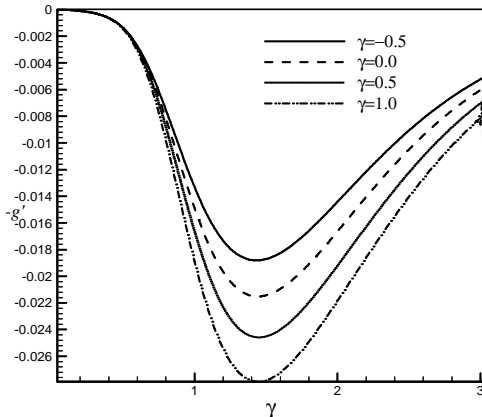


Fig. 34: Effect of γ on Skin friction coefficient in z -direction.

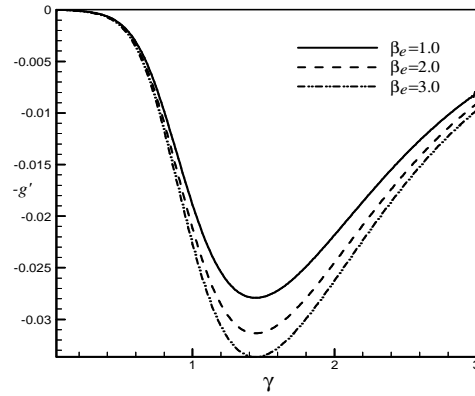


Fig. 37: Effect of β_e on Skin friction coefficient in z -direction.

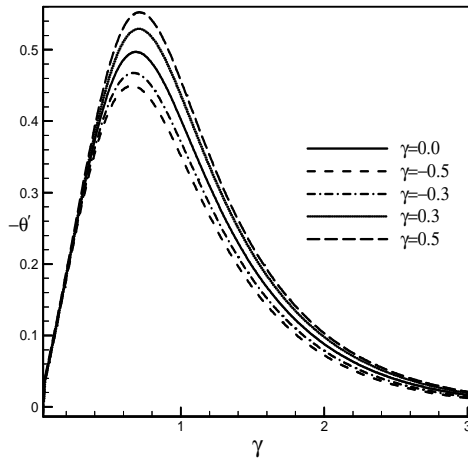


Fig. 35: Effect of γ on the rate of heat transfer.

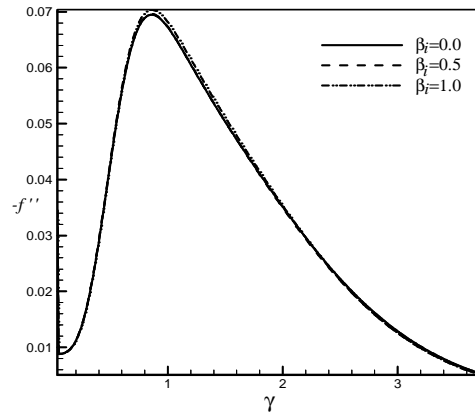


Fig. 38: Effect of β_e on the rate of heat transfer.

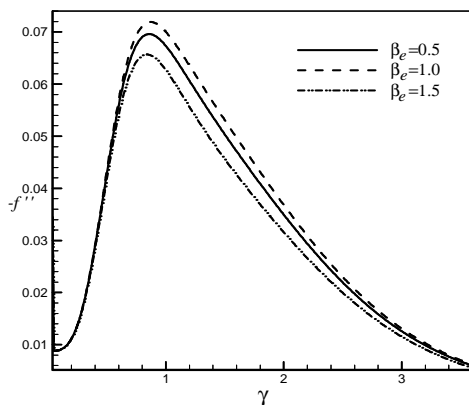


Fig. 36: Effect of β_e on Skin friction coefficient in x -direction.

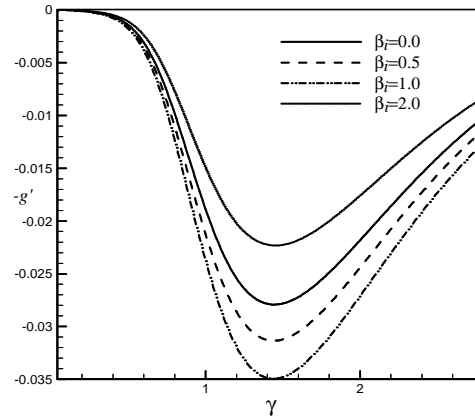


Fig. 39: Effect of β_i on Skin friction coefficient in z -direction.

MHD Free-Convection from a Rotating Vertical Plate with Power-law Variation

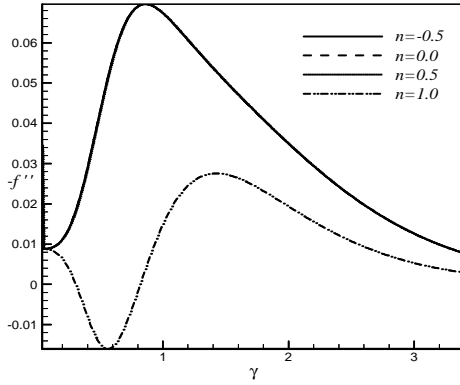


Fig. 40: Effect of n on Skin friction coefficient in x -direction.

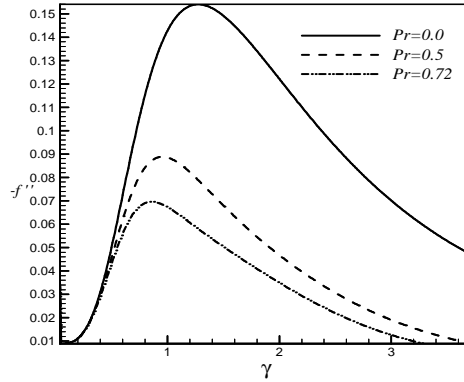


Fig. 43: Effect of P_r on Skin friction coefficient in x -direction

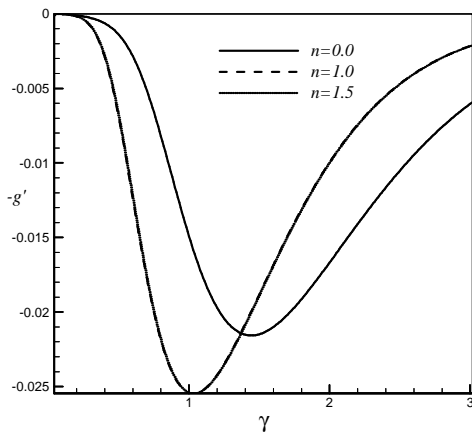


Fig. 41: Effect of n on Skin friction coefficient in z -direction.

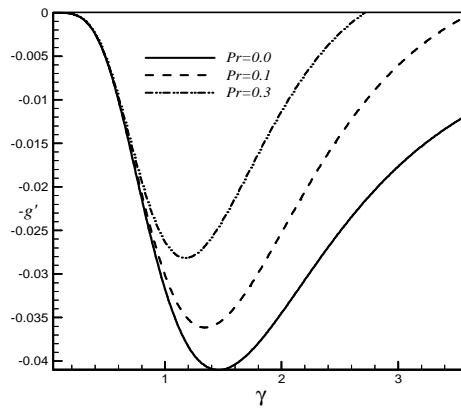


Fig. 44: Effect of P_r on Skin friction coefficient in z -direction.

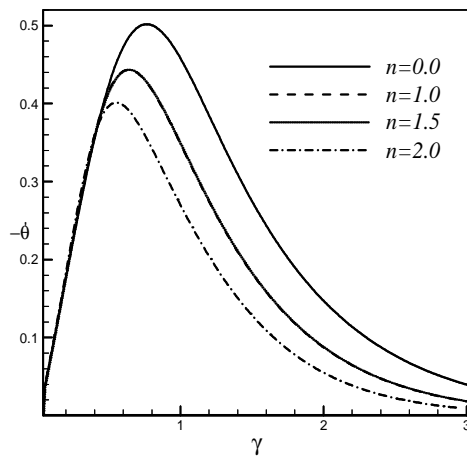


Fig. 42: Effect of n on the rate of heat transfer.

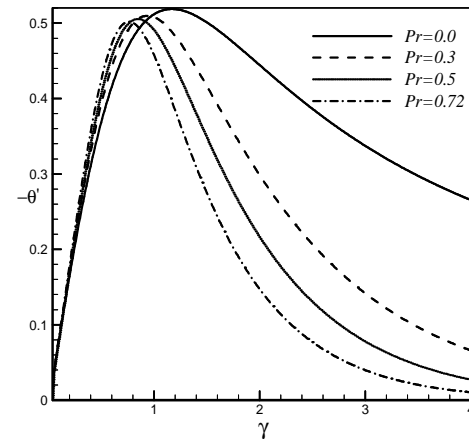


Fig. 45: Effect of P_r on the rate of heat transfer.

6. Conclusion

The important findings of the investigation from graphical representation are listed below:

1. The primary velocity decreases with the increases of M , R , β_i and P_r while the secondary velocity increases with the increase of M , β_i , P_r , Ec , γ and n .
2. The secondary velocity decreases with the increases of R and β_e while the primary velocity increases with the increase of γ , β_e and n .
3. The temperature profiles increases with the increase of M and R while it decreases with the increase of P_r , γ and n .
4. Shear stress in x -direction increases for γ and decreases for M , β_i , P_r , Ec , R and n .
5. Shear stress in z -direction increases for increasing M , P_r , n and decreases with the increase of β_e , γ and R .
6. Nusselt number increases with the increase of R and γ while decreases with the increase P_r and n .

REFERENCES

1. E.M.Sparrow and R.D.Cess, The effect of a magnetic field on free convection heat transfer, *Int. J. Heat Mass Transfer*, 3 (1961) 267-274.
2. M.A.Hossain, Viscous and Joule heating effects on MHD free-convection flow with variable plate temperature, *International Journal of Heat and Mass Transfer*, 35(12) (1992) 3485-3487.
3. E.M.Abo-Eldahab and M.A.Aziz, Viscous dissipation and joule heating effects on MHD-free convection from a vertical plate with power-law variation in surface temperature in the presence of Hall and ion-slip currents, *Applied Mathematical Modeling*, 29 (2005) 579-595.
4. Md. Kutub Uddin, Rabindra Nath Mondal, "Md. Sharif Uddin and Sanjit Kumar Paul, A numerical study on radiation-conduction interaction with steady streamwise surface temperature variations over a vertical cone, *Annals of Pure and Applied Mathematics*, 2(2) (2012) 151-163
5. M. M. Haque, M. S. Uddin, M. A. Islam and M. H. Uddin, Ekman boundary layer mixed convective heat transfer flow through a porous medium with large suction, *Annals of Pure and Applied Mathematics*, 3(1) (2013) 17-26.
6. Md. Saidul Islam, Md. Samsuzzoha, Shamim Ara and Pinakee Dey, MHD free convection and mass transfer flow with heat generation through an inclined plate, *Annals of Pure and Applied Mathematics*, 3(2) (2013) 129-141.